




## Open Archive Toulouse Archive Ouverte (OATAO)

OATAO is an open access repository that collects the work of Toulouse researchers and makes it freely available over the web where possible

This is a Publisher's version published in: <http://oatao.univ-toulouse.fr/21004>

**Official URL:** <https://doi.org/10.1103/PhysRevMaterials.1.064002>

### To cite this version:

Zubair, Ahmed and Tristant, Damien and Nie, Chunyang and Tsentalovich, Dmitri E. and Headrick, Robert J. and Pasquali, Matteo and Kono, Junichiro and Meunier, Vincent and Flahaut, Emmanuel and Monthieux, Marc  and Gerber, Iann C. and Puech, Pascal *Charged iodide in chains behind the highly efficient iodine doping in carbon nanotubes*. (2017) *Physical Review Materials*, 1 (6). 1-7. ISSN 2475-9953

Any correspondence concerning this service should be sent to the repository administrator: [tech-oatao@listes-diff.inp-toulouse.fr](mailto:tech-oatao@listes-diff.inp-toulouse.fr)

## Charged iodide in chains behind the highly efficient iodine doping in carbon nanotubes

Ahmed Zubair,<sup>1</sup> Damien Tristant,<sup>2,3,4</sup> Chunyang Nie,<sup>3,5</sup> Dmitri E. Tsentalovich,<sup>6</sup> Robert J. Headrick,<sup>6,7</sup> Matteo Pasquali,<sup>6,7,8</sup> Junichiro Kono,<sup>1,8,9</sup> Vincent Meunier,<sup>2</sup> Emmanuel Flahaut,<sup>10</sup> Marc Monthieux,<sup>3</sup> Yann C. Gerber,<sup>4</sup> and Pascal Puech<sup>3,\*</sup>

<sup>1</sup>Department of Electrical and Computer Engineering, Rice University, Houston, Texas 77005, USA

<sup>2</sup>Department of Physics, Applied Physics, and Astronomy, Rensselaer Polytechnic Institute, Troy, New York 12180, USA

<sup>3</sup>CEMES-CNRS, UPR-8011, Université Fédérale de Toulouse-Midi-Pyrénées, Toulouse, France

<sup>4</sup>LPCNO, UMR-5215 CNRS, INSA, Université Fédérale de Toulouse-Midi-Pyrénées, Toulouse, France

<sup>5</sup>School of Environmental Science and Engineering, Guangdong University of Technology, Guangzhou, 510006, P. R. China

<sup>6</sup>Department of Chemical and Biomolecular Engineering, Rice University, Houston, Texas 77005, USA

<sup>7</sup>Department of Chemistry, Rice University, Houston, Texas 77005, USA

<sup>8</sup>Department of Materials Science and NanoEngineering, Rice University, Houston, Texas 77005, USA

<sup>9</sup>Department of Physics and Astronomy, Rice University, Houston, Texas 77005, USA

<sup>10</sup>Institut Carnot CIRIMAT, Université Fédérale de Toulouse-Midi-Pyrénées, UMR CNRS 5085, Toulouse, France

(Received 26 September 2017; published 27 November 2017)

The origin of highly efficient iodine doping of carbon nanotubes is not well understood. Relying on first-principles calculations, we found that iodine molecules ( $I_2$ ) in contact with a carbon nanotube interact to form monoiodide or/and polyiodide from two and three  $I_2$  as a result of removing electrons from the carbon nanotube ( $p$ -type doping). Charge per iodine atom for monoiodide ion or iodine atom at end of iodine chain is significantly higher than that for  $I_2$ . This atomic analysis extends previous studies showing that polyiodide ions are the dominant dopants. Moreover, we observed isolated I atoms in atomically resolved transmission electron microscopy, which proves the production of monoiodide. Finally, using Raman spectroscopy, we quantitatively determined the doping level and estimated the number of conducting channels in high electrical conductivity fibers composed of iodine-doped double-wall carbon nanotubes.

DOI: 10.1103/PhysRevMaterials.1.064002

### I. INTRODUCTION

Single-wall, double-wall, and multiwall carbon nanotubes (SWCNTs, DWCNTs, and MWCNTs, respectively) are quasi-one-dimensional materials that have the structure of rolled-up graphene sheets [1–5]. Individual Carbon nanotubes (CNTs) have some extraordinary properties such as ultrahigh electrical and thermal conductivity [6,7], light weight and high mechanical strength [8], which make them promising for various applications, including solar energy [9], electronics [10], and biomedical technology [11]. However, these excellent properties often drastically diminish in macroscopic form, e.g., films, sheets, fibers, ropes, wires, and cables of CNTs. Recently, reports on doped CNT fibers [12–14] have revealed ultrahigh electrical conductivity. These macroscopic fibers are a candidate for replacement of metals as a universal conducting wire and will have a wide range of applications, such as aeronautics, space, power transmission, and automobile industry [15].

Iodine ( $I_2$ ) is known to be an efficient dopant for CNTs, but the doping mechanism is not well understood. Recent *ab initio* calculations of graphene doping by iodine suggested that various iodine species should be considered [16,17]. Even though many characterization studies have been conducted on doping processes in CNTs [18–20], the mechanism of iodine doping remains a long-debated subject. Tri-iodide ( $I_3^-$ ) and penta-iodide ( $I_5^-$ ), which are easily observable by Raman scattering, have been reported to be at the origin of doping [21], but the large conductance enhancement observed is not

in agreement with the charge carrier concentration estimated by first-principles calculations. Moreover, monoiodide ions ( $I^-$ ) have been observed with Mössbauer spectroscopy with a large charge transfer for iodine doping of CNTs [22].

In this work, we try to explain the great gain of conductivity associated with iodine doping. We first start our study by first-principles calculations. We unambiguously demonstrate the formation of chain of charged iodide and the corresponding low-energy cost for the creation of monoiodide. Then, by studying Raman spectroscopy in DWCNTs well-purified assembled in fibers and doped with iodine, and compared with calculations performed on SWCNTs associated with I and TEM images obtained on iodine chains encapsulated in moderately purified DWCNTs.

### II. METHODS

#### A. First-principles calculations

We performed first-principles calculations based on density functional theory (DFT). The structural and electronic properties of CNT systems were obtained with the Vienna *ab initio* simulation package (VASP) [23–26]. The plane-wave basis set cutoff energy was set to be 400 eV with a Gaussian smearing method of 0.005 eV width, in order to ensure well-converged total energy and force values. To properly account for van der Waals interactions, we used the OPTB86B-VDW scheme [27], based on previous work on carbon-based systems [16]. All atoms were allowed to relax until the maximum of forces acting on them became smaller than  $0.01 \text{ eV } \text{Å}^{-1}$ .

These calculations were performed for iodine-filled (7,7) and (9,9) SWCNTs and also for (7,7), (9,9), (11,11), (13,13),

\*Corresponding author: pascal.puech@cemes.fr

and (15,15) SWCNT bundles containing iodine between nanotubes. We also added the case of (10,10)@(15,15) DWCNTs which correspond to CNTs in doped fibers. Initial SWCNT geometries were generated by the TUBEGEN code [28]. The calculated supercell ( $1 \times 1 \times 10$ ) used for both isolated SWCNTs and SWCNT bundles contained four iodine atoms. For the case of (11,11) SWCNT bundle containing six iodine atoms, a supercell ( $1 \times 1 \times 14$ ) was used. For the isolated SWCNT, we used a separation of 3 and 5 nm in two perpendicular directions with respect to the CNT axis direction for (7,7) and (9,9) SWCNT systems, respectively, in order to avoid interaction between two adjacent periodic structures. For the SWCNT bundle, a hexagonal lattice was used. The  $k$ -point sampling was always based on a  $\Gamma$ -centered grid for all types of calculations. A ( $1 \times 1 \times 2$ ) grid and a ( $2 \times 2 \times 2$ ) grid were used to optimize isolated CNT and a CNT bundle system, respectively. Then, a ( $1 \times 1 \times 5$ ) grid and a ( $5 \times 5 \times 5$ ) grid were used to determine the charge transfer of an isolated CNT and a CNT bundle, respectively. Bader charge analysis was carried out using Henkelman's Group program [29–31].

For comparison, we also calculated the adsorption energy of eight adsorption sites of an  $I_2$  molecule adsorbed on two different CNTs: a (7,7) metallic armchair and a (11,0) semiconducting zigzag CNTs, with a small diameter (around 0.9 nm). Since no significant changes were observed, with adsorption energy difference lower than 0.01 eV, we performed all our energy studies on metallic systems. In a previous work of Tristant *et al.* [32] (main text and electronic supplemental information), we also analyzed the case of highly doped CNTs with large diameter and found a similar Fermi level shift for both semiconducting and metallic CNTs.

To fill the CNTs, oxidation allows iodine going inside. On the contrary, to obtain high conductive CNTs fiber, the CNTs should be free of defects to have a large electronic mean-free path and, therefore, no oxidation is present. Consequently, in our scenarios, the case of having both situations was disregarded, not for technical difficulties but as it did not correspond to our samples.

### B. Iodine-doped CNT-fiber production

The CNT fibers used in this study were produced from well-purified DWCNTs (residual catalyst content less than 5% and no amorphous residue) by the wet-spinning process reported by Behabtu *et al.* [12]. During the manufacturing process, these fibers were doped inherently by chlorosulfonic acid. We later annealed the fibers to remove the doping species originating from the superacid according to the method in Ref. [12]. Such annealed (and thus close to pristine) fibers were then kept in an iodine vapor chamber for 24 h at 200 °C to ensure a high degree of doping.

### C. Raman spectroscopy

Raman spectroscopy experiments were performed at room temperature with a 568-nm excitation wavelength laser using a T64000 Jobin-Yvon Horiba spectrometer in a backscattering configuration on an iodine-doped CNT fiber. The laser power was kept below 0.4 mW, and the laser beam was focused onto the sample with an objective lens with a magnification of  $\times 40$ .

### D. Electrical conductivity measurements

For electrical conductivity measurements of iodine-doped fibers, we used a home-built nitrogen-purged transport measurement system. We used a square U-shaped epoxy glass substrate to suspend the fiber. We used a four-terminal configuration: silver paste was used to make contact between the fiber and gold wires, which were connected to the connection pins of a cryostat sample holder. We placed the sample on the cryostat sample holder that was kept in a vacuum-sealed chamber. The chamber was initially pumped down to a few tenths of pascal, and then nitrogen gas was introduced into the chamber. We followed a similar procedure to that described by Xuan *et al.* [13] for current-carrying capacity measurements. Current through the fiber was swept up at a certain value (which was increased by step at each cycle) and then swept back to 1 mA. The resistance of the sample was continuously recorded during the current sweeping cycles. The current value was increased until the fiber broke. We measured the diameter of fibers using an optical microscope.

### E. Transmission electron microscopy

For transmission electron microscopy (TEM) experiments, another set of samples was prepared [33,34] for which iodine from the vapor phase was introduced inside DWCNTs (midly purified, with HCl only in order to remove the excess of catalyst Co nanoparticles) in order to observe the arrangement of the iodine atoms clearly. First, dry, raw DWCNTs along with iodine rocks were ground in a mortar together to obtain a homogeneous mixture. The mixture was transferred into a quartz ampoule. The ampoule was sealed and placed into a furnace. The furnace temperature was slowly (5 °C/min) ramped up to 827 °C and kept at 827 °C for 24 h and then slowly (0.1 °C/min between 827 °C to 777 °C and 1 °C/min down to room temperature) ramped down to room temperature. Once the heating process was completed, the ampoule was taken out of the furnace, and the composite powder taken out from the ampoule was ground into a fine powder. The powder was washed with ethanol to dissolve the residual iodine. To prepare a TEM specimen, the iodine-filled DWCNT samples were dispersed in ethanol using a sonication bath. Then, a few drops of suspension were deposited onto a copper grid (200 mesh) coated with a lacey-type carbon film using a glass pipette. After the evaporation of the ethanol from the grid, the specimen was ready for observation. These iodine-filled DWCNTs were imaged by a JEOL JEM-ARM200F microscope (200 KV) equipped with a STEM and Cs corrector for the condenser lens.

## III. RESULTS AND DISCUSSION

### A. First-principles calculations

To find if the mechanism at the origin of the ultrahigh conductivity is the activation of electronic channels due to the large Fermi level shift originating from iodine doping, we considered the interaction between two iodine molecules and CNT walls to form charged species from charge transfer. Since the dissociation of a single  $I_2$  on graphene is clearly unfavorable (+0.74 eV) [17], more molecules should be considered. First, we calculated interaction of four iodine atoms inside a SWCNT and between SWCNTs inside a

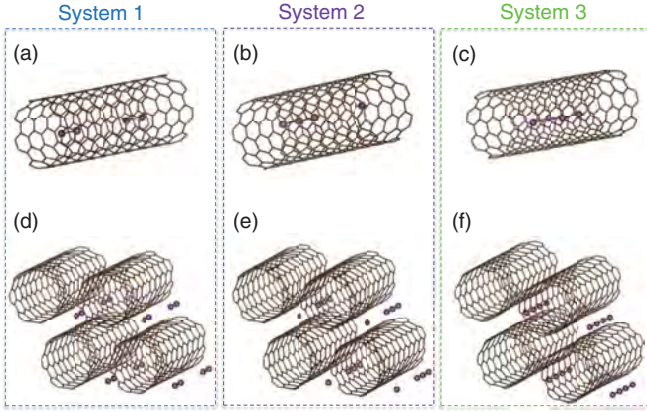


FIG. 1. View of the different intercalation sites of (a)  $I_2$ , (b)  $I_3^{\delta_3^-} + I^{\delta_1^-}$ , and (c)  $I_4^{\delta_4^-}$  inside a (7,7) SWCNT, (d)  $2I_2$ , (e)  $I_3^{\delta_3^-} + I^{\delta_1^-}$ , and (f)  $I_4^{\delta_4^-}$  on a (7,7) SWCNT bundle.

bundle. To compare the energy stability between system 1 ( $2I_2 + \text{SWCNT}$ ) and system 2 ( $I_3^{\delta_3^-} + I^{\delta_1^-} + \text{SWCNT}^{\delta_{\text{CNT}^+}}$ ), where  $\delta$  is the estimated charge transfer, we used the following equation:

$$\Delta E = E_{\text{system}_2} - E_{\text{system}_1}, \quad (1)$$

and the same approach for system 3 ( $I_4^{\delta_4^-} + \text{CNT}^{\delta_{\text{CNT}^+}}$ ).

Both configurations, iodine filling the SWCNT and iodine in the SWCNT bundle, of systems 1, 2, and 3 are illustrated in Fig. 1. The energy difference  $\Delta E$  values of doped CNT systems are shown in Table I. For the chiralities of (7,7) and (9,9), the tube diameter is 0.95 and 1.22 nm, respectively. The interaction of  $2I_2$  leads to a reduction of energy for iodine atoms inside CNTs and iodine atoms in the CNT bundle. Insertion or adsorption configurations help stabilize the monoiodide and tri-iodide as well as the tetraiodide. Tetraiodide is more favorable, but the energy difference is not large enough to be the unique species at room temperature. In order to know if tetraiodide is always the more stable configuration, we calculated the energy difference between systems 2 and 3 for diameters up to 2 nm. We also considered the systems 2 and 3 for (10,10)@(15,15) DWCNT bundle. For large diameter tubes, we noted that the cylinders become deformed due to van der Waals interaction. The energy difference is reported in Fig. 2. For a diameter larger than 1.4 nm, the energy difference is constant and close to 0.2 eV.

TABLE I. Energy difference between systems 2 and 1 and 3 and 1 (eV), for the doped-inside isolated SWCNT and the doped SWCNT bundle. The first values are from the (7,7) SWCNT systems and the values between parentheses are from the (9,9) SWCNT systems.

	System	$\Delta E$ (eV)
Inside	1 ( $I_2$ )	
	2 ( $I_3^{\delta_3^-} + I^{\delta_1^-}$ )	-0.68
	3 ( $I_4^{\delta_4^-}$ )	-0.76
Bundle	1 ( $I_2$ )	
	2 ( $I_3^{\delta_3^-} + I^{\delta_1^-}$ )	-0.83(-0.67)
	3 ( $I_4^{\delta_4^-}$ )	-1.41(-1.08)

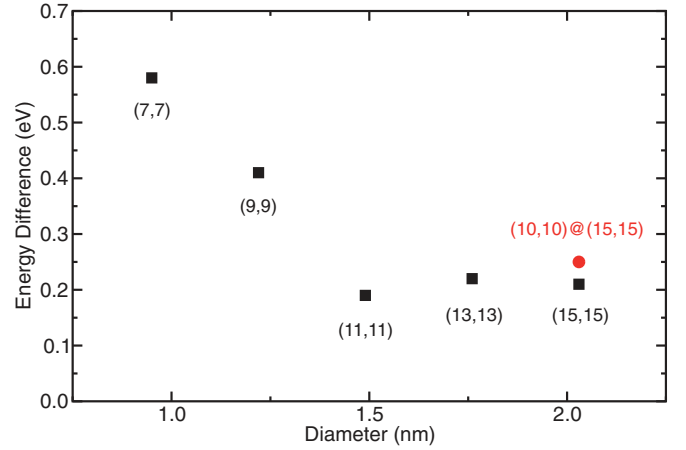


FIG. 2. Energy difference (eV) between  $I_3^{\delta_3^-} + I^{\delta_1^-}$  and  $I_4^{\delta_4^-}$  for (7,7), (9,9), (11,11), (13,13), (15,15) SWCNT bundles and (10,10)@(15,15) DWCNT bundles. The  $I_4^{\delta_4^-}$  CNT system remains the most energetically stable. 0.2 eV corresponds to 2300 K.

This value is quite small and can be viewed as an accurate estimate of the energy barrier for the transformation of  $I_4$  to  $I_3+I$ . Indeed, our attempt to estimate the transition state using nudged elastic band type of calculations on the (9,9) bundle from  $I_4$  to  $I_3+I$  configurations provide us a late transition state of less than 10 meV higher than the  $I_3+I$  energy.

The bond lengths between iodine atoms of  $I_2$ ,  $I_3^{\delta_3^-}$ , and  $I_4^{\delta_4^-}$  species, for the doped-inside isolated SWCNT and the doped SWCNT bundle, are shown in Table II. The bond lengths in  $I_3^{\delta_3^-}$  and  $I_4^{\delta_4^-}$  are longer than that of  $I_2$  (2.72 Å). The bond length increase is correlated to the charge transfer on each atom forming the bond.

The estimated charge transfer values are summarized in Table III. The value of  $\delta$  is connected to the modification of the I-I bond length (see Table II and Fig. 3). There is no charge transfer when  $I_2$  is in a CNT bundle as it is a stable state for iodine. But, charge transfer happens when di-iodide is inside CNTs. The bond length increase is due to electron transfer from the CNT to the iodine. These results indicate that the diameter of CNTs plays a significant role towards the stability of iodine species when iodine fills the CNTs. Most importantly, the charge per iodine atom for monoiodide is much higher than for other species which agrees with the

TABLE II. The bond distance (in Å) between iodine atoms belonging to  $I_2$ ,  $I_3^{\delta_3^-}$ , and  $I_4^{\delta_4^-}$  species, for the doped inside isolated SWCNTs and the doped SWCNT bundles. The first values are from the (7,7) SWCNT systems and the values between parentheses are from (9,9) SWCNT systems.

	Species	Bond length (Å)
Inside	$I_2$	2.87
	$I_3^{\delta_3^-}$	[2.98 2.98]
	$I_4^{\delta_4^-}$	[3.12 2.99 3.13]
Bundle	$I_2$	2.72(2.71)
	$I_3^{\delta_3^-}$	[2.88 2.89]([2.89 2.89])
	$I_4^{\delta_4^-}$	[3.12 2.86 3.13]([3.21 2.85 3.15])

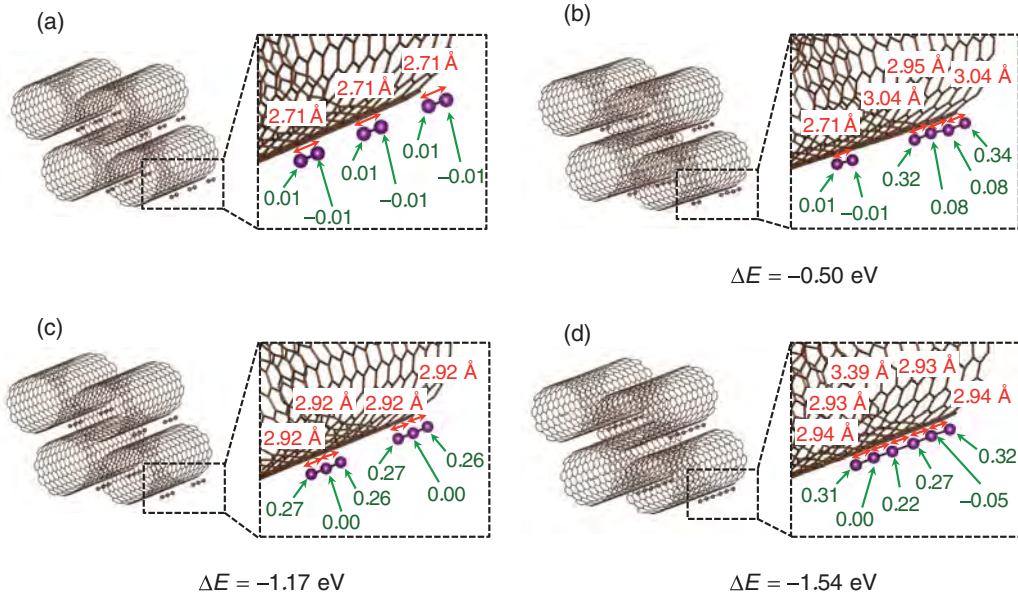


FIG. 3. View of the different intercalation sites of (a)  $3I_2$ , (b)  $I_4^{\delta_4^-} + I_2$ , (c)  $2I_3^{\delta_3^-}$ , and (d)  $I_6^{\delta_6^-}$  on a (11,11) SWCNT bundle with their bond length (red color) and charge transfer per atom (green color). Energy difference  $\Delta E$  between  $3I_2$  and other systems is provided. The  $I_6^{\delta_6^-}$  CNT system is the most energetically stable.

Mössbauer finding [22]. For the bundle, the doping due to this process is also really large and consistent with the high electrical conductivity reached by the iodine-doped DWCNT fiber, as described in latter paragraphs.

To extend our study to larger polyiodine chains, as observed experimentally, we calculated four configurations involving up to six iodine atoms:  $3I_2$ ,  $I_4^{\delta_4^-} + I_2$ ,  $2I_3^{\delta_3^-}$ , and  $I_6^{\delta_6^-}$ . In Fig. 3, the configuration as well as the bond length and the charge transfer for each iodine atom are reported. The iodine atoms at the ends of each iodide species account for the highest amount of charges. The  $I_6^{\delta_6^-}$  is the most stable but the bond length in the middle is very large and this configuration is close to  $2I_3^{\delta_3^-}$ . Interestingly, a clear distinction in the type of polyiodides seems difficult because the charge transfer for each atom within a chain is different. The charge is not fully delocalized over all atoms. The bond length is directly related to the charge of each atom constituting it. Mind that in these calculations, we completely neglect temperature effects (0 K calculations) and large fluctuations of bond lengths may arise from higher temperatures.

### B. Transmission electron microscopy

Using TEM, we observed the arrangement of the iodine atoms filling the inner cavity of DWCNTs (Fig. 4). The annular

TABLE III. Transferred charge per iodide ion species  $\delta$ , for the iodine-doped-inside isolated SWCNT and the doped SWCNT bundle. The first value is for the (7,7) SWCNT, and the value between parentheses is for the (9,9) SWCNT.

	$I_1^{\delta_1^-}$	$I_3^{\delta_3^-}$	$I_2^{\delta_2^-}$	$I_4^{\delta_4^-}$
$\delta$ Inside	0.64	0.84	0.33	1.11
Bundle	0.32(0.39)	0.38(0.50)	0.00(0.00)	0.68(0.88)

dark field image from TEM clearly shows that iodine is able to form encapsulated linear chains inside DWCNTs exhibiting the suitable inner diameter [35]. As the annular dark field is highly sensitive to variations in the atomic number of atoms in the sample, iodine atoms, with atomic number 53, are much brighter than carbon atoms from the CNTs. Hence, the CNT are hardly seen. In Fig. 4, we can see bright dots, each corresponding to iodine atom, and forming chains. There are two such iodine chains inside two DWCNTs in the figure. Monoiodides and polyiodides can be found in this TEM image. We indicated the occurrence of monoiodides using white solid arrows and that of tri-iodide with white, dashed arrows. The interaction between  $I_2$  molecules that subsequently leads to the formation of ion species with a high doping density is therefore further ascertained by both our calculations and atomically resolved TEM image.

### C. Electrical conductivity

To determine the conductivity increase due to iodine doping, we measured the current-carrying capacity of the iodine-doped fibers. Iodine-doped fibers had a conductivity of  $6.5 \pm 0.1 \times 10^6 \text{ S m}^{-1}$ , which is higher than that of chlorosulfonic

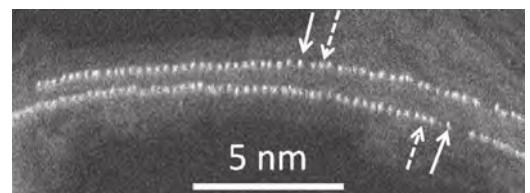


FIG. 4. TEM images of iodine-filled DWCNTs. Two chains of iodine inside two DWCNTs are shown here. White, solid arrows show the presence of monoiodide species, and white, dashed arrows show the presence of tri-iodide species.

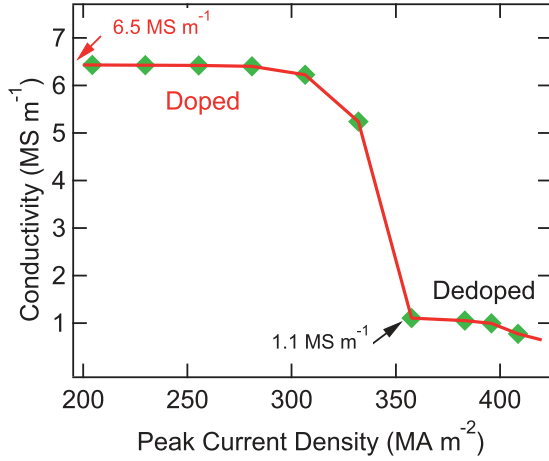


FIG. 5. Plot of the conductivity values measured after a current-sweeping cycle as a function of applied peak current density used for the cycling series.

acid-doped fibers [32]. From Fig. 5, we can see that at low current densities (below  $330 \text{ MA m}^{-2}$ ), the conductivity of the iodine-doped fiber remains constant. Above a threshold value of current density (above  $360 \text{ MA m}^{-2}$ ) in cyclic conditions [13], spontaneous dedoping of the fiber occurs due to Joule effect (at a temperature around  $110 \pm 30^\circ\text{C}$ ), resulting in a sudden drop in conductivity. The conductivity decreases by about 6, corresponding to the removal of iodine dopants. We repeated this experiment several times, and the conductivity drop factor was confirmed to always be in the range of 5 to 7.

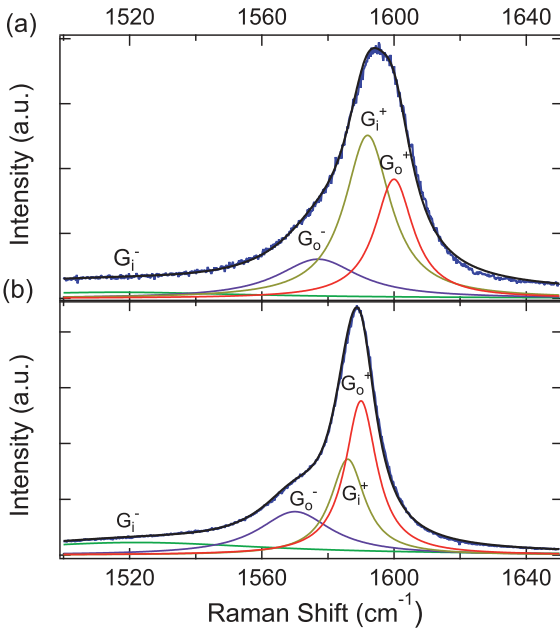


FIG. 6. Raman spectra in the  $G$ -band regime of (a) iodine-doped and (b) dedoped fibers. The blue and black solid lines represent experimental and theoretical fits data, respectively. The green, purple, brown, and red solid lines represent the  $G_i^-$ ,  $G_o^-$ ,  $G_i^+$ , and  $G_o^+$  peaks, respectively.

TABLE IV. Raman shift,  $\omega$  ( $\text{cm}^{-1}$ ), and FWHM ( $\text{cm}^{-1}$ ) of fitted four Lorentzian peaks for Raman spectra of the doped and dedoped fibers. We estimated uncertainty for  $\omega$  and FWHM to be lower than  $1 \text{ cm}^{-1}$  (1%).

		$G_i^-$	$G_o^-$	$G_i^+$	$G_o^+$
Doped fiber	$\omega$ ( $\text{cm}^{-1}$ )	1516	1577	1592	1600
	FWHM ( $\text{cm}^{-1}$ )	100	29.8	16.8	14.0
Dedoped fiber	$\omega$ ( $\text{cm}^{-1}$ )	1522	1570	1586	1590
	FWHM ( $\text{cm}^{-1}$ )	100	26.9	12.5	11.6

#### D. Raman spectroscopy

To determine the doping level, we acquired Raman spectra on both iodine-doped and dedoped fibers. Figure 6 shows the Raman  $G$  bands of (a) an iodine-doped DWCNT fiber and (b) a dedoped DWCNT fiber, fit with four Lorentzians. We previously described how this decomposition analysis provides information on doping [32]. These four peaks represent the upper ( $G^+$ ) and lower ( $G^-$ ) branches of the inner ( $G_i$ ) and outer ( $G_o$ ) tube characteristics of the  $G$  band of DWCNTs. Table IV summarizes the frequencies ( $\omega$ ) and full width at half maximum (FWHM) of the four Lorentzian peaks.  $G_o^-$ ,  $G_i^+$ , and  $G_o^+$  of the iodine-doped fiber were blue-shifted compared to the dedoped fiber.

The  $G$ -band shift associated with the inner tube is due to the lattice contraction of the outer tube. From the  $6 \text{ cm}^{-1}$  shift of the  $G_i^+$  bands between the doped and dedoped fibers, we estimated the shift due to bond contraction for the outer tube to be  $1.7 \times 6 = 10 \text{ cm}^{-1}$  (the factor 1.7 comes from strain transmission between the outer and inner tubes [36]). This value corresponds to the shift of the  $G_o^+$  band between the doped and dedoped fibers. Therefore, we can conclude that no adiabatic effect is present based on the formulation in our previous work [32]. From this shift, it is possible to estimate the charge transfer factor per carbon atom:  $f_C = 10/350 = 0.029$  and, then, the average Fermi level shift by  $\langle \Delta E_F \rangle_N = 6.04\sqrt{f_C} = 1 \text{ eV}$ , a relation that is only valid for very large doping ( $f_C > 0.007$ ) [32].

Due to the high level of doping, there are multiple conductance channels that are occupied by charge carriers. To estimate the number of conducting channels, a full calculation could be done as in our previous work [32], but a rough estimation is also possible using  $E_i(\text{eV}) = (\gamma_0 a_{C-C} i)/d = 0.38i/d(\text{nm})$ [37] (metallic  $i = 0, 3, 6, \dots$ , semiconducting  $i = 1, 2, 4, 5, 7, 8, \dots$ ). Before doping, a statistical analysis gives  $\frac{1}{3}$  metallic (2 channels) and  $\frac{2}{3}$  semiconducting (0 channel) for inner and outer tubes. The number of conducting channels for a DWCNT is  $\frac{4}{3}$  on average. As the outer diameter is  $\sim 2 \text{ nm}$ , by moving the average Fermi level by  $1 \text{ eV}$ , we obtain  $i \approx 5$ ; thus, outer semiconducting and metallic tubes are more conductive (6 and 6 channels, respectively). Assuming weak charge transfer for the inner tube (no modification), the number of conducting channels for a doped DWCNT is  $\frac{26}{3}$  on average. Hence, the conductance improvement is about  $\frac{26}{4} = 6.5$ .

As the length of the fiber is macroscopic, our experiments were conducted only in the diffusive transport regime. Thus, the mean-free path of the electrons should be considered. As

the density of defects is low [12], the mean-free path is not altered by the shift of the Fermi level and remains nearly constant (31 nm for the iodine-doped fiber and 33 nm for the dedoped fiber). As a matter of fact, only the diffusive regime is considered in the literature [38].

#### IV. CONCLUSIONS

The high level of conductivity in iodine-doped CNTs is due not only to  $I_3^{\delta_3^-}$  and  $I_5^{\delta_5^-}$  polyiodine ions, but also to  $I^{\delta_1^-}$  and  $I_4^{\delta_4^-}$  species. Charge variation along a  $I_6^{\delta_6^-}$  chain looks like the association of two  $I_3^{\delta_3^-}$ . Due to variation of the charge transfer along the chain, the species are not clearly separable but their number are larger than when considering only triiodides and pentaiodides. Using DFT, we determined how 2 and  $3I_2$  interact. Monoiodide can be formed through the reaction  $2I_2 + CNT \rightarrow I^{\delta_1^-} + I_3^{\delta_3^-} + CNT^{\delta_{CNT}^+}$  even if the reaction  $2I_2 + CNT \rightarrow I_4^{\delta_4^-} + CNT^{\delta_{CNT}^+}$  is energetically more stable with a moderate energy difference (0.2 eV) for CNTs with large diameters. Charge transferred from  $I^{\delta_1^-}$  or iodine atoms at the ends of a iodine chain to CNT is strikingly higher than that from  $I_2$  to CNT. In an iodine-doped DWCNT fiber, the charge transfer factor  $f_C$  is close to 0.03. As a consequence,

the increased number of conducting channels explains the conductivity increase by a factor of 6. Iodine doping is enough to explain the conductivity improvement. As the density of defects is low, the conduction is not altered by the shift of the Fermi level in the CNTs. Iodine doping is enough to explain the conductivity improvement.

#### ACKNOWLEDGMENTS

This work was supported by Programme Investissements d'Avenir under the Program No. ANR-11-IDEX-0002-02, Reference No. ANR-10-LABX-0037-NEXT, by the Robert A. Welch Foundation (USA), Grants No. C-1509 and No. C-1668, by the W. M. Keck Foundation (USA), by NASA Space Technology Research Fellowship (NSTRF14) number NNX14AL71H, by the Department Of Energy (DOE) award DEEE0007865, and by Air Force Office of Scientific Research Grant No. FA9550-15-1-0370. Theoretical calculations were performed using CALMIP (Project No. p0812) and HPC resources from GENCI-IDRIS, GENCI-Curie, and GENCI-Occigen (Project No. x2016096649).

- 
- [1] S. Iijima, *Nature (London)* **354**, 56 (1991).  
 [2] S. Iijima and T. Ichihashi, *Nature (London)* **363**, 603 (1993).  
 [3] D. Bethune, C. H. Kiang, M. De Vries, G. Gorman, R. Savoy, J. Vazquez, and R. Beyers, *Nature (London)* **363**, 605 (1993).  
 [4] N. Hamada, S.-i. Sawada, and A. Oshiyama, *Phys. Rev. Lett.* **68**, 1579 (1992).  
 [5] R. Pfeiffer, C. Kramberger, F. Simon, H. Kuzmany, V. Popov, and H. Kataura, *Eur. Phys. J. B* **42**, 345 (2004).  
 [6] C. T. White and T. N. Todorov, *Nature (London)* **393**, 240 (1998).  
 [7] P. Poncharal, C. Berger, Y. Yi, Z. L. Wang, and W. A. de Heer, *J. Phys. Chem. B* **106**, 12104 (2002).  
 [8] M. J. Treacy, T. Ebbesen, and J. Gibson, *Nature (London)* **381**, 678 (1996).  
 [9] K. Suzuki, M. Yamaguchi, M. Kumagai, and S. Yanagida, *Chem. Lett.* **32**, 28 (2002).  
 [10] F. Mirri, A. W. Ma, T. T. Hsu, N. Behabtu, S. L. Eichmann, C. C. Young, D. E. Tsentalovich, and M. Pasquali, *ACS Nano* **6**, 9737 (2012).  
 [11] A. Bianco, K. Kostarelos, C. D. Partidos, and M. Prato, *Chem. Commun.* **571** (2005).  
 [12] N. Behabtu, C. C. Young, D. E. Tsentalovich, O. Kleinerman, X. Wang, A. W. K. Ma, E. A. Bengio, R. F. ter Waarbeek, J. J. de Jong, R. E. Hoogerwerf *et al.*, *Science* **339**, 182 (2013).  
 [13] X. Wang, N. Behabtu, C. C. Young, D. E. Tsentalovich, M. Pasquali, and J. Kono, *Adv. Funct. Mater.* **24**, 3241 (2014).  
 [14] A. Zubair, D. E. Tsentalovich, C. C. Young, M. S. Heimbeck, H. O. Everitt, M. Pasquali, and J. Kono, *Appl. Phys. Lett.* **108**, 141107 (2016).  
 [15] M. F. De Volder, S. H. Tawfick, R. H. Baughman, and A. J. Hart, *Science* **339**, 535 (2013).  
 [16] D. Tristant, P. Puech, and I. C. Gerber, *J. Phys. Chem. C* **119**, 12071 (2015).  
 [17] R. A. Hoyt, E. M. Remillard, E. D. Cubuk, C. D. Vecitis, and E. Kaxiras, *J. Phys. Chem. C* **121**, 609 (2016).  
 [18] R. Österbacka, C. P. An, X. Jiang, and Z. V. Vardeny, *Science* **287**, 839 (2000).  
 [19] A. M. Rao, P. Eklund, S. Bandow, A. Thess, and R. E. Smalley, *Nature (London)* **388**, 257 (1997).  
 [20] T. Michel, L. Alvarez, J.-L. Sauvajol, R. Almairac, R. Aznar, O. Mathon, J.-L. Bantignies, and E. Flahaut, *J. Phys. Chem. Solids* **67**, 1190 (2006).  
 [21] G. Kalita, K. Wakita, M. Takahashi, and M. Umeno, *J. Mater. Chem.* **21**, 15209 (2011).  
 [22] S. Kitao, M. Seto, Y. Kobayashi, R. Haruki, S. Masubuchi, S. Kazama, H. Kataura, Y. Maniwa, S. Suzuki, and Y. Achiba, *Hyperfine Interactions* (Springer, Berlin, 2002), pp. 67–70.  
 [23] G. Kresse and J. Hafner, *Phys. Rev. B* **47**, 558 (1993).  
 [24] G. Kresse and J. Hafner, *Phys. Rev. B* **49**, 14251 (1994).  
 [25] G. Kresse and J. Furthmüller, *Phys. Rev. B* **54**, 11169 (1996).  
 [26] G. Kresse and J. Furthmüller, *Comput. Mater. Sci.* **6**, 15 (1996).  
 [27] J. Klimeš, D. R. Bowler, and A. Michaelides, *Phys. Rev. B* **83**, 195131 (2011).  
 [28] J. T. Frey and D. J. Doren, University of Delaware, Newark DE, USA, 2011.  
 [29] G. Henkelman, A. Arnaldsson, and H. Jónsson, *Comput. Mater. Sci.* **36**, 354 (2006).  
 [30] E. Sanville, S. D. Kenny, R. Smith, and G. Henkelman, *J. Comput. Chem.* **28**, 899 (2007).  
 [31] W. Tang, E. Sanville, and G. Henkelman, *J. Phys.: Condens. Matter* **21**, 084204 (2009).  
 [32] D. Tristant, A. Zubair, P. Puech, F. Neumayer, S. Moyano, R. J. Headrick, D. E. Tsentalovich, C. C. Young, I. C. Gerber, M. Pasquali *et al.*, *Nanoscale* **8**, 19668 (2016).

- [33] C. Nie, A.-M. Galibert, B. Soula, E. Flahaut, J. Sloan, and M. Monthioux, *Carbon* **110**, 48 (2016).
- [34] E. Flahaut, R. Bacsa, A. Peigney, and C. Laurent, *Chem. Commun.* 1442 (2003).
- [35] C. Nie, A.-M. Galibert, B. Soula, L. Datas, J. Sloan, E. Flahaut, and M. Monthioux, *Carbon* **16**, 759 (2017).
- [36] P. Puech, E. Flahaut, A. Sapelkin, H. Hubel, D. J. Dunstan, G. Landa, and W. S. Bacsa, *Phys. Rev. B* **73**, 233408 (2006).
- [37] J. W. Mintmire and C. T. White, *Phys. Rev. Lett.* **81**, 2506 (1998).
- [38] J.-C. Charlier, X. Blase, and S. Roche, *Rev. Mod. Phys.* **79**, 677 (2007).